Reversal Mechanism of an Individual Ni Nanotube Simultaneously Studied by Torque and SQUID Magnetometry

A. Buchter,[1] J. Nagel,[2] D. Rüffer,[3] F. Xue (薛飞),[1] D. P. Weber,[1] O. F. Kieler,[4] T. Weimann,[4] J. Kohlmann,[4]
A. B. Zorin,[4] E. Russo-Averchi,[3] R. Huber,[5] P. Berberich,[5] A. Fontcuberta i Morral,[3] M. Kemmler,[2]
R. Kleiner,[2] D. Koelle,[2] D. Grundler,[5,6,*] and M. Poggio[1,†]

[1]*Department of Physics, University of Basel, 4056 Basel, Switzerland*
[2]*Physikalisches Institut and Center for Collective Quantum Phenomena in LISA+, Universität Tübingen, 72076 Tübingen, Germany*
[3]*Laboratoire des Matériaux Semiconducteurs, Institut des Matériaux, Ecole Polytechnique Fédérale de Lausanne,
1015 Lausanne, Switzerland*
[4]*Fachbereich 2.4 "Quantenelektronik", Physikalisch-Technische Bundesanstalt, 38116 Braunschweig, Germany*
[5]*Lehrstuhl für Physik funktionaler Schichtsysteme, Physik Department E10,
Technische Universität München, 85747 Garching, Germany*
[6]*Institut des Matériaux, Faculté Sciences et Technique de l'Ingénieur, Ecole Polytechnique Fédérale de Lausanne,
1015 Lausanne, Switzerland*

Using an optimally coupled nanometer-scale SQUID, we measure the magnetic flux originating from an individual ferromagnetic Ni nanotube attached to a Si cantilever. At the same time, we detect the nanotube's volume magnetization using torque magnetometry. We observe both the predicted reversible and irreversible reversal processes. A detailed comparison with micromagnetic simulations suggests that vortexlike states are formed in different segments of the individual nanotube. Such stray-field free states are interesting for memory applications and noninvasive sensing.

Recent experimental and theoretical work has demonstrated that nanometer-scale magnets, as a result of their low dimensionality, display magnetic configurations not present in their macroscopic counterparts [1–3]. Such work is driven by both fundamental questions about nanometer-scale magnetism and the potential for applying nanomagnets as elements in high-density memories [4], in high-resolution imaging [5–7], or as magnetic sensors [8]. Compared to nanowires, ferromagnetic nanotubes are particularly interesting for magnetization reversal as they avoid the Bloch point structure [9]. Different reversal processes via curling, vortex wall formation, and propagation have been predicted [10–13]. Because of their inherently small magnetic moment, experimental investigations have often been conducted on large ensembles. The results, however, are difficult to interpret due to stray-field interactions and the distribution in size and orientation of the individual nanotubes [12,14–18]. In a pioneering work, Wernsdorfer *et al.* [19] investigated the magnetic reversal of an individual Ni nanowire at 4 K using a miniaturized SQUID. Detecting the stray magnetic flux Φ from one end of the nanowire as a function of magnetic field **H**, Φ was assumed to be approximately proportional to the projection of the total magnetization **M** along the nanowire axis. At the time, $M(H)$ of the individual nanowire was not accessible and micromagnetic simulations were conducted only a decade later [9]. Here, we present a technique to simultaneously measure $\Phi(H)$ and $M(H)$ of a single low-dimensional magnet. Using a scanning nanoSQUID and a cantilever-based torque magnetometer

(Fig. 1) [20], we investigate a Ni nanotube producing $\Phi(H)$ with a nearly square hysteresis, similar to the Ni nanowire of Ref. [19]. $M(H)$, however, displays a more complex behavior composed of reversible and irreversible contributions, which we interpret in detail with micromagnetic simulations. In contrast to theoretical predictions, the experiment suggests that magnetization reversal is not initiated from both ends. If nanomagnets are to be optimized for storage or sensing applications, such detailed investigations of nanoscale properties are essential.

We use a direct current nanoSQUID formed by a loop containing two superconductor-normal-superconductor Josephson junctions (JJs) [21–23] [Fig. 1(a)]. Two T-shaped superconducting Nb arms are sputtered on top of each other separated by an insulating layer of SiO_2. The Nb arms are connected via two planar 225 nm thick Nb/HfTi/Nb JJs each with an area of 200×200 nm^2. These JJs and the 1.8 μm long Nb leads form a SQUID loop in the xz plane [shown in yellow in Fig. 1(a)], through which we measure Φ. Atomic layer deposition of Ni is used to prepare the nanotube around a GaAs nanowire template grown by molecular beam epitaxy [24,25]. The GaAs core supports the structure, making it mechanically robust. The polycrystalline nanotube, which does not exhibit magneto-crystalline anisotropy, has a 140 ± 20 nm outer diameter, a 70 ± 10 nm inner diameter, and a 6.0 ± 0.5 μm length. The error in the diameters results from the roughness of the Ni film [23]. The Ni nanotube is affixed to the end of an ultrasoft Si cantilever [25], such
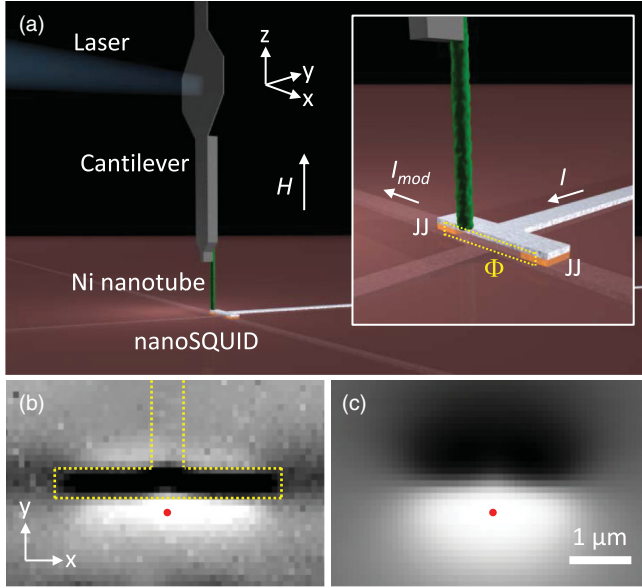
FIG. 1 (color).   (a) Sketch of the apparatus (inset: zoomed-in view; dashed line indicates SQUID loop). Gray-scale maps of (b) $\Delta f(x, y)$ and (c) $\Phi(x, y)$ taken simultaneously at a distance $z = 280$ nm with $H = 0$. Δf (Φ) ranges from -170 to 430 Hz (-0.08 to $0.08\Phi_0$). Dashed lines indicate the T-shaped SQUID arm and dots the operating position.

that it protrudes from the tip by 4 μm. The cantilever is 120 μm long, 4 μm wide and 0.1 μm thick. It hangs above the nanoSQUID in the pendulum geometry, inside a vacuum chamber (pressure $< 10^{-6}$ mbar) at the bottom of a cryostat. A 3D piezoelectric positioning stage moves the nanoSQUID relative to the Ni nanotube and an optical fiber interferometer is used to detect deflections of the cantilever along $\hat{y}$ [26]. Fast and accurate measurement of the cantilever's fundamental resonance frequency f_c is realized by self-oscillation at a fixed amplitude. An external field $\mu_0\mathbf{H}$ of up to 2.8 T can be applied along the cantilever axis $\hat{z}$ using a superconducting magnet. At 4.3 K and $\mu_0 H = 0$, the cantilever, loaded with the Ni nanotube and far from any surfaces, has an intrinsic resonance frequency $f_c = f_0 = 3413$ Hz, a quality factor $Q = Q_0 = 3.4 \times 10^4$, and spring constant of $k_0 = 90 \pm 10$ μN/m. The magnetic flux due the Ni nanotube $\Phi_{\mathrm{NN}}(H)$ is evaluated from $\Phi_{\mathrm{NN}}(H) = \Phi(H) - \Phi_{\mathrm{ref}}(H)$, where the flux $\Phi(H)$ is measured with the nanotube close to the nanoSQUID, while $\Phi_{\mathrm{ref}}(H)$ is measured with the nanotube several μm away such that the stray flux is negligible. Therefore, $\Phi_{\mathrm{ref}}(H) \propto H$, due to the small fraction of $\mathbf{H}$ that couples through the nanoSQUID given its imperfect alignment with $\hat{z}$. Once calibrated, we also use $\Phi_{\mathrm{ref}}(H)$ to measure the $\mu_0 H$ axis of our plots, removing effects due to hysteresis in the superconducting magnet. Such a field calibration was not possible for the integrated SQUID of Ref. [19]. We also perform dynamic-mode cantilever magnetometry [27], which is sensitive to the dynamic component of the magnetic torque acting between $\mathbf{H}$ and the

magnetization $\mathbf{M}$ of the Ni nanotube. In order to extract $M(H)$, we measure the field-dependent frequency shift $\Delta f(H) = f_c(H) - f_0$. Micromagnetic simulations are performed with NMAG [28] which provides finite-element modeling by adapting a mesh to the curved inner and outer surfaces of the nanotube. We simulate 30 nm thick nanotubes of different lengths l and the same 70 nm inner diameter. We assume magnetically isotropic Ni consistent with earlier studies [24], a saturation magnetization $M_S = 406$ kA/m [29], and an exchange coupling constant of 7×10^{12} J/m [30].

We first scan the nanoSQUID under the cantilever with the attached Ni nanotube, to map the coupling between them. To ensure that the scan is done with the nanotube in a well-defined magnetic state, we first saturate it along its easy axis ($\hat{z}$). Scans are then made at $H = 0$ in the xy plane at a fixed height z, i.e., for a fixed distance between the top of the SQUID device and the bottom end of the Ni nanotube. $\Delta f(x, y) = f_c(x, y) - f_0$ and $\Phi(x, y)$ are measured simultaneously, as shown in Figs. 1(b) and 1(c), respectively. $\Delta f(x, y)$ is proportional to the force gradient $\partial F_y/\partial y$ acting on the cantilever and is sensitive to both the topography of the sample and to the magnetic field profile in its vicinity. Raised features such as the T-shaped top-electrode of the nanoSQUID are visible. $\Phi(x, y)$ shows a bipolar flux response. The change in sign of $\Phi(x, y)$ occurs as the Ni nanotube crosses the xz plane (defined by the SQUID loop) above the nanoSQUID, matching the expected response. Such images allow us to identify the nanoSQUID and to position the Ni nanotube at a maximum of $|\Phi(x, y)|$. Given a constant z, the nanotube stray flux optimally couples through the nanoSQUID loop at such positions, resulting in the maximum signal-to-noise ratio for flux measurements.

At one such position, indicated by the dot in Fig. 1, we record $\Phi(H)$ by sweeping $\mu_0 H$ from 41 to -41 mT and vice versa. A representative hysteresis curve $\Phi_{\mathrm{NN}}(H) = \Phi(H) - \Phi_{\mathrm{ref}}(H)$ is shown in Fig. 2(a) where $\Phi(H)$ is measured at $z = 450$ nm. $\mu_0 |H|$ is incremented in steps of 0.2 mT with a wait time of 1 s before each acquisition. The hysteresis has an almost square shape with a maximum flux $\Phi_{\mathrm{NN}} = 75$ mΦ_0 coupled into the nanoSQUID. The loop appears similar to stray-field hysteresis loops obtained from a bistable Ni nanomagnet [31] and the Ni nanowire of Ref. [19], where H was collinear with the long axis. Such a shape may suggest that at $H = 0$ the remanent magnetization $M_R \approx M_S$. Increasing H from zero [see red branch in Fig. 2(a)], we first observe a nearly constant flux, then a variation by about 30% along with tiny jumps in a small field regime, and finally, a large jump occurring near 30 mT. Similar to Ref. [19], our SQUID data suggest that almost all magnetic moments are reversed at once near 30 mT via a large irreversible jump, i.e., via domain nucleation and propagation.

We now turn to cantilever magnetometry, which is sensitive to $M(H)$. Δf is first measured simultaneously with
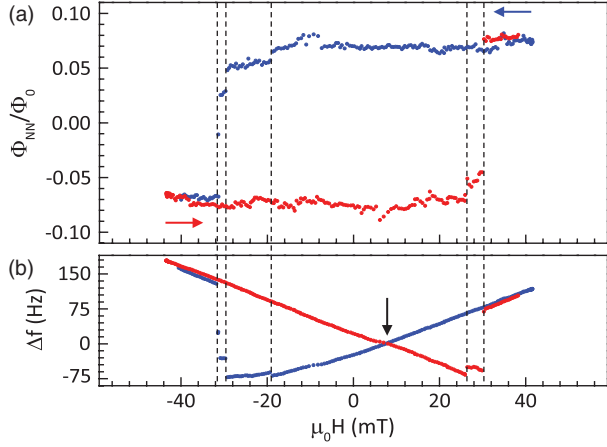
FIG. 2 (color). Simultaneously measured hysteresis loops of
(a) $\Phi_{NN}(H)$ and (b) $\Delta f(H)$ at $z = 450$ nm. Red (blue) points
represent data taken while sweeping H in the positive (negative)
direction. Dashed lines indicate discontinuities (magnetic
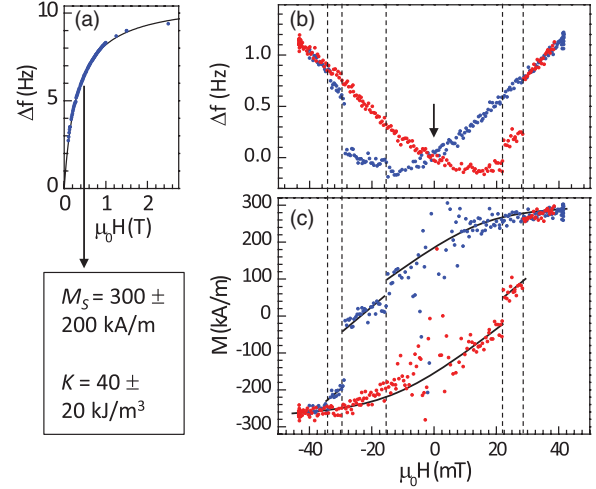switching fields $H_{sw,e}$) appearing in both $\Phi_{NN}(H)$ and $\Delta f(H)$.

FIG. 3 (color). (a) Cantilever magnetometry (points) and fit
(solid line) in large magnetic fields. (b) Cantilever magnetometry
at small fields. (c) Volume magnetization M extracted from
(b) according to (1). Solid lines guide the eye. Red (blue) points
represent data taken while sweeping H in the positive (negative)
direction. Dashed lines highlight switching fields $H_{sw,e}$. The
error in M scales with $1/|H|$, explaining the scatter near $H = 0$.

$\Phi(H)$ at $z = 450$ nm, as shown in Fig. 2(b). The torque
measured via Δf is found to exhibit tiny jumps and large
abrupt changes at exactly the same switching fields $H_{sw,e}$
as $\Phi_{NN}(H)$. We note that switching fields vary from sweep
to sweep [23] as was observed in the Ni nanowire of
Ref. [19]; such behavior is expected if nucleation is
involved, given its stochastic nature. Importantly, there is
always a one-to-one correspondence between switching
fields observed in Δf and flux Φ_{NN} as highlighted by the
dashed lines in Fig. 2. This correlation confirms that the
changes in Δf and Φ_{NN} have a single origin: the reversal of
magnetic moments within the Ni nanotube.

In order to analyze $\Delta f(H)$ in terms of $M(H)$, it is
important to retract the Ni nanotube from the
nanoSQUID by several μm. Therefore, we avoid magnetic
interactions with both the diamagnetic superconducting
leads and the modulation current of the nanoSQUID.
These interactions lead to an enhanced Δf and a branch
crossing [indicated by an arrow in Fig. 2(b)] occurring at
finite H rather than at $H = 0$ as was reported in Ref. [24].
After retracting the nanotube from the nanoSQUID, we
measure $\Delta f(H) = f_c(H) - f_0$ as shown in Fig. 3. We start
the acquisition at a large positive field ($\mu_0 H = 2.8$ T),
where the nanotube is magnetized to saturation, and then
reduce H to zero as shown in Fig. 3(a). In large fields, the
nanotube behaves as a single-domain magnetic particle;
i.e., it is magnetized uniformly and M rotates in unison as
the cantilever oscillates in the magnetic field. Based on this
assumption, we fit the results with an analytical model for
$\Delta f(H)$ [25]. The volume of the Ni nanotube V_{Ni}, ω_0, and
k_0 are set to their measured values, while the saturation
magnetization $M_S = 300 \pm 200$ kA/m and the anisotropy
parameter $K = 40 \pm 20$ kJ/m^3 are extracted as fit parame-
ters. The error in these parameters is dominated by the
error associated with the measurement of the nanotube's

exact geometry and therefore of V_{Ni} [23]. M_S is consistent
with the findings of Ref. [25] on similar nanotubes and
with 406 kA/m, known as the saturation magnetization for
bulk crystalline Ni at low temperature [29].

Figure 3(b) shows $\Delta f(H)$ taken in the low-field regime.
In an opposing field, we observe discrete steps in $\Delta f(H)$
indicating abrupt changes in the volume magnetization M.
As expected, the branch crossing (arrow) occurs at $H = 0$
and the overall behavior is consistent with measurements
of similar nanotubes [25]. To analyze the low field data,
we adapt the analytical model to extract the dependence of
the volume magnetization M on H, i.e., the field depen-
dence of magnetization averaged over the entire volume of
the nanotube. Solving the equations of Ref. [25] describing
the frequency shift for M, we find

$$M = \frac{2k_0 l_e^2 K \Delta f}{H(KV_{Ni}f_0 - k_0 l_e^2 \Delta f)}, \qquad (1)$$

where $l_e = 85$ μm is the effective cantilever length for
the fundamental mode. $M(H)$ extracted from Fig. 3(b) is
plotted in Fig. 3(c). In both field sweep directions, the
magnetization is seen to first undergo a gradual decrease
as $|H|$ decreases. Starting from ~300 kA/m at +40 mT,
M reduces to ~200 kA/m at 0 mT. We find $M_R \approx 0.65$ M_S,
in contrast with the SQUID data suggesting $M_R \approx M_S$.
However, this gradual change of M at small $|H|$ in the
initial stage of the reversal is consistent with the gradually
changing anisotropic magnetoresistance observed in a
similar nanotube of larger diameter in nearly the same field
regime [24]. At -15 mT, just before the first of three
discontinuous jumps, M is only ~100 kA/m. Note that

jumps are seen after the magnetization has decreased to a value of about $0.3M_S$. Two further jumps occur at $\mu_0 H_{sw,e} = -28$ and -33 mT. For $\mu_0 H < -40$ mT, the nanotube magnetization is completely reversed. We observe a somewhat asymmetric behavior at positive and negative fields. This asymmetry may be due to an antiferromagnetic NiO surface layer providing exchange interaction with the Ni nanotube [32,33]. Irreversible jumps in M are observed for 15 mT $< \mu_0|H_{sw,e}| < 35$ mT in Fig. 3, in perfect agreement with the range over which jumps occur in Φ_{NN} with the nanotube close to the nanoSQUID in Fig. 2.

The observed magnetization steps suggest the presence of 2 to 4 intermediate magnetic states or 2 to 4 segments in the nanotube that switch at different H. Calculations for ideal nanotubes [10] suggest that the intermediate states should be multidomain, consisting of uniform axially saturated domains separated by azimuthal or vortexlike domain walls. The preferred sites for domain nucleation are expected to be the two ends of the nanotube [9,10]. As the field is reduced after saturation, magnetic moments should gradually curl or tilt away from the field direction. The torque magnetometry measurements, which show both gradual and abrupt changes in $M(H)$, are consistent with such gradual tilting; the SQUID data, showing only abrupt changes in $\Phi_{NN}(H)$, are not. In the following, we present micromagnetic simulations performed on Ni nanotubes of different lengths l to further analyze our data.

In Fig. 4(a), we show simulated hysteresis loops $M(H)$ with **H** applied along the long axis of nanotubes with l between 250 nm and 2 μm. For $l = 2$ μm the $M(H)$ loop is almost square, but the switching field is ~ 8 mT. This value is much smaller than the regime of $H_{sw,e}$ observed experimentally. Nanotubes with 250 nm $< l <$ 1 μm are consistent with 15 mT $< \mu_0|H_{sw,e}| < 35$ mT. For $l = 500$ nm the simulation provides a switching field $\mu_0 H_{sw} = 28$ mT. At the same time, M is almost zero for $|H|$ just below $|H_{sw}|$. Such behavior is consistent with the overall shape of the measured $M(H)$ loop in Fig. 3(c), where the largest jumps in M take place at about ± 30 mT. Comparing Figs. 4(a) and 3(c), we conclude that the superposition of a few segments with 250 nm $< l < 1$ μm could account for the measured $M(H)$. For such segments, Figs. 4(b) and 4(c) (right panels) show characteristic spin configurations (cones) well above and near H_{sw}, respectively. We observe the gradual tilting of spins at both ends in Fig. 4(b) and two tubularlike vortex domains with opposite circulation direction in Fig. 4(c) [34]. Between the domains, a Néel-type wall exists. For each l and $M(H)$, we simulate the relevant stray field at the position of the nanoSQUID [red squares in the left panels of Figs. 4(b) and 4(c)] providing the predicted $\Phi_{NN}(H)$ [23]. The shapes of the simulated $\Phi_{NN}(H)$ are nearly proportional to, and thus closely follow, the shape of $M(H)$ shown in Fig. 4(a). Thus, the simulations allow us to explain the measured torque magnetometry data, although they are inconsistent with the nanoSQUID data.
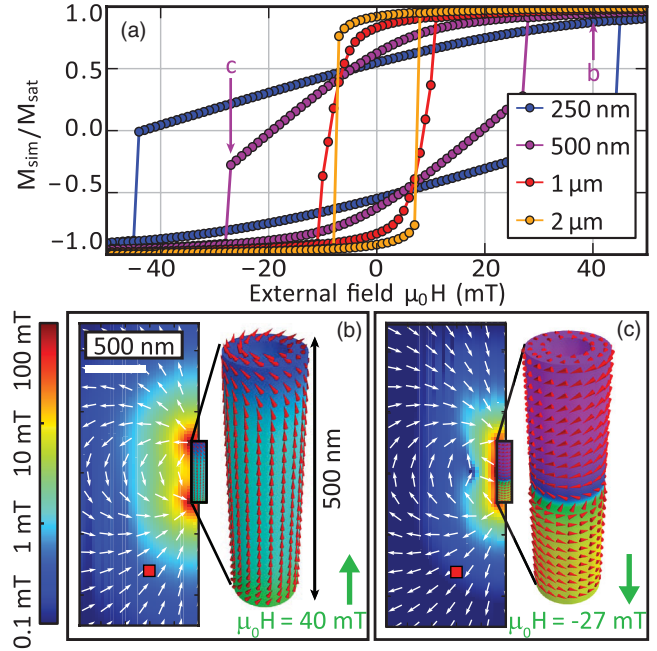

FIG. 4 (color).   (a) Simulated hysteresis loops $M(H)$ for nanotubes of four different l. H_{sw} increases with decreasing l. Magnetic configurations (right) and stray-field distribution (left) for $l = 500$ nm at (b) 40 mT and (c) -27 mT as indicated by the labels in (a). Cones (arrows) indicate the local direction of the magnetic moments (stray field). The stray fields H_{str} are color coded as depicted. The red squares indicate the position of the center of the nanoSQUID loop.

The contrast between hysteresis traces obtained by the nanoSQUID and torque magnetometry shows that $\Phi(H)$ is not the projection of **M** along the nanotube axis. This finding contradicts the assumption of Ref. [19]; we attribute this discrepancy to the fact that while cantilever magnetometry measures the entire volume magnetization, the nanoSQUID is most sensitive to the magnetization at the bottom end of the nanotube, as shown in calculations of the coupling factor $\phi_\mu = \Phi/\mu$ (flux Φ coupled to nanoSQUID by a pointlike particle with magnetic moment μ) [20]. Still, we find a one-to-one correspondence between switching fields $H_{sw,e}$ detected by either the nanoSQUID or cantilever magnetometry. This experimentally verified consistency substantiates the reversal field analysis performed in Ref. [19]. In Fig. 2(a), we find no clear evidence for curling or gradual tilting at small H. Thus, the reversal process does not seem to start from the end closest to the nanoSQUID, but rather from a remote segment. This is an important difference compared to the ideal nanotubes considered thus far in the literature, in which both ends share the same fate in initiating magnetization reversal. The unintentional roughness of real nanotubes might be relevant here. In an experiment performed on a large ensemble of nanotubes, one would not have been able to judge whether a gradual decrease in $M(H)$ [17] originated from a very broad switching field distribution

or from the gradual tilting of magnetic moments in the individual nanotubes. Thus, our combination of nanomagnetometry techniques represents a powerful method for unraveling hidden aspects of nanoscale reversal processes. In order to optimize nanotubes for sensing and memory applications, such understanding is critical.

In summary, we have presented a technique for measuring magnetic hysteresis curves of nanometer-scale structures using a piezoelectrically positioned nanoSQUID and a cantilever operated as a torque magnetometer. This dual functionality provides two independent and complementary measurements: one of local stray magnetic flux and the other of volume magnetization. Using this method we gain microscopic insight into the reversal mechanism of an individual Ni nanotube, suggesting the formation of vortexlike tubular domains with Néel-type walls.

*grundler@ph.tum.de
†martino.poggio@unibas.ch

[1] Z. K. Wang, M. H. Kuok, S. C. Ng, D. J. Lockwood, M. G. Cottam, K. Nielsch, R. B. Wehrspohn, and U. Gösele, Phys. Rev. Lett. **89**, 027201 (2002).

[2] R. Streubel, J. Thurmer, D. Makarov, F. Kronast, T. Kosub, V. Kravchuk, D. D. Sheka, Y. Gaididei, R. Schäfer, and O. G. Schmidt, Nano Lett. **12**, 3961 (2012).

[3] R. Streubel, V. P. Kravchuk, D. D. Sheka, D. Makarov, F. Kronast, O. G. Schmidt, and Y. Gaididei, Appl. Phys. Lett. **101**, 132419 (2012).

[4] S. S. P. Parkin, M. Hayashi, and L. Thomas, Science **320**, 190 (2008).

[5] S. Khizroev, M. H. Kryder, D. Litvinov, and D. A. Thompson, Appl. Phys. Lett. **81**, 2256 (2002).

[6] M. Poggio and C. L. Degen, Nanotechnology **21**, 342001 (2010).

[7] H. Campanella, M Jaafar, J. Llobet, J. Esteve, M. Vázquez, A. Asenjo, R. P. del Real, and J. A. Plaza, Nanotechnology **22**, 505301 (2011).

[8] M. M. Maqableh, X. Huang, S.-Y. Sung, K. S. M. Reddy, G. Norby, R. H. Victora, and B. J. H. Stadler, Nano Lett. **12**, 4102 (2012).

[9] R. Hertel and J. Kirschner, J. Magn. Magn. Mater. **278**, L291 (2004).

[10] P. Landeros, O. J. Suarez, A. Cuchillo, and P. Vargas, Phys. Rev. B **79**, 024404 (2009).

[11] P. Landeros and Á. S. Núñez, J. Appl. Phys. **108**, 033917 (2010).

[12] J. Escrig, J. Bachmann, J. Jing, M. Daub, D. Altbir, and K. Nielsch, Phys. Rev. B **77**, 214421 (2008).

[13] P. Landeros, S. Allende, J. Escrig, E. Salcedo, D. Altbir, and E. E. Vogel, Appl. Phys. Lett. **90**, 102501 (2007).

[14] J. Bachmann, J. Jing, M. Knez, S. Barth, H. Shen, S. Mathur, U. Gösele, and K. Nielsch, J. Am. Chem. Soc. **129**, 9554 (2007).

[15] M. Daub, M. Knez, U. Goesele, and K. Nielsch, J. Appl. Phys. **101**, 09J111 (2007).

[16] J. Bachmann, J. Escrig, K. Pitzschel, J. M. Montero Moreno, J. Jing, D. Görlitz, D. Altbir, and K. Nielsch, J. Appl. Phys. **105**, 07B521 (2009).

[17] O. Albrecht, R. Zierold, S. Allende, J. Escrig, C. Patzig, B. Rauschenbach, K. Nielsch, and D. Görlitz, J. Appl. Phys. **109**, 093910 (2011).

[18] J. Escrig, S. Allende, D. Altbir, and M. Bahiana, Appl. Phys. Lett. **93**, 023101 (2008).

[19] W. Wernsdorfer, B. Doudin, D. Mailly, K. Hasselbach, A. Benoit, J. Meier, J.-Ph. Ansermet, and B. Barbara, Phys. Rev. Lett. **77**, 1873 (1996).

[20] J. Nagel, A. Buchter, F. Xue, O. F. Kieler, T. Weimann, J. Kohlmann, A. B. Zorin, D. Rüffer, E. Russo-Averchi, R. Huber, P. Berberich, A. Fontcuberta i Morral, D. Grundler, R. Kleiner, D. Koelle, M. Poggio, and M. Kemmler, arXiv:1305.1195.

[21] J. Nagel, O. F. Kieler, T. Weimann, R. Wölbing, J. Kohlmann, A. B. Zorin, R. Kleiner, D. Koelle, and M. Kemmler, Appl. Phys. Lett. **99**, 032506 (2011).

[22] R. Wölbing, J. Nagel, T. Schwarz, O. Kieler, T. Weimann, J. Kohlmann, A. Zorin, M. Kemmler, R. Kleiner, and D. Koelle, Appl. Phys. Lett. **102**, 192601 (2013).

[23] See Supplemental Material at http://link.aps.org/supplemental/10.1103/PhysRevLett.111.067202 for a description of the experimental methods, further flux hysteresis loops, discussion of the simulations, and a description of the detection of simultaneous switching events.

[24] D. Rüffer, R. Huber, P. Berberich, S. Albert, E. Russo-Averchi, M. Heiss, J. Arbiol, A. Fontcuberta i Morral, and D. Grundler, Nanoscale **4**, 4989 (2012).

[25] D. P. Weber, D. Rüffer, A Buchter, F. Xue, E. Russo Averchi, R. Huber, P. Berberich, J. Arbiol, A. Fontcuberta i Morral, D. Grundler, and M. Poggio, Nano Lett. **12**, 6139 (2012).

[26] D. Rugar, H. J. Mamin, and P. Guethner, Appl. Phys. Lett. **55**, 2588 (1989).

[27] B. C. Stipe, H. J. Mamin, T. D. Stowe, T. W. Kenny, and D. Rugar, Phys. Rev. Lett. **86**, 2874 (2001).

[28] T. Fischbacher, M. Franchin, G. Bordignon, and H. Fangohr, IEEE Trans. Magn. **43**, 2896 (2007); http://nmag.soton.ac.uk/nmag/.

[29] C. Kittel, *Introduction to Solid-State Physics* (Wiley, New York, 2005), 8th ed.

[30] A. Knittel, Ph.D. thesis, University of Southampton, 2011.

[31] G. Meier, D. Grundler, K.-B. Broocks, Ch. Heyn, and D. Heitmann, J. Magn. Magn. Mater. **210**, 138 (2000).

[32] P. Zhang, F. Zuo, F. K. Urban III, A Khabari, P. Griffiths, and A. Hosseini-Tehrani, J. Magn. Magn. Mater. **225**, 337 (2001).

[33] M. Gierlings, M. J. Prandolini, H. Fritzsche, M. Gruyters, and D. Riegel, Phys. Rev. B **65**, 092407 (2002).

[34] A.-P. Chen, J. M. Gonzalez, and K. Y. Guslienko, J. Appl. Phys. **109**, 073923 (2011).